

NOTICE: this is the author's version of a work that was accepted for publication in International Journal of Solids and Structures. Changes resulting from the publishing process, such as peer review, editing, corrections, structural formatting, and other quality control mechanisms may not be reflected in this document. Changes may have been made to this work since it was submitted for publication. A definitive version was subsequently published in International Journal of International Journal of Solids and Structures, Volume 48, Issue 9, May 2011. DOI:10.1016/j.ijsolstr.2011.01.010

# **Residual stresses in multi-layered silicon-on-sapphire thin film systems**

A. Pramanik, L.C. Zhang<sup>1</sup>,

School of Mechanical and Manufacturing Engineering, The University of New South

Wales, NSW 2052, Australia

## **Abstract**

This paper uses the finite element method to analyse the dynamic process of residual stress generation and variation in silicon-on-sapphire thin film systems during cooling. The effects of material properties, thin film structures and processing conditions, on the stress distribution were explored in detail. It was found that under certain conditions, significant stress concentration and discontinuity can take place to initiate crack and/or delamination in the systems. However, these can be minimised by controlling the buffer layer thickness.

**Keywords:** Multi-layered, thin film, residual stress, buffer layer, cooling

---

<sup>1</sup> Corresponding author. Tel.: +612 9385 6078; fax: +612 9385 7316  
Email address: Liangchi.Zhang@unsw.edu.au

## **1. Introduction**

Multi-layered thin film systems have been used in a broad range of fields such as in optical, electronic, mechanical and protective applications (McCann, 2001, Mylvaganam, 2003, Pramanik, 2008a, Richmond, 1982). The hetero-epitaxial process is used to generate multi-layered thin films of a semiconductor material, such as silicon, on insulated sapphire substrates for electronic circuits. The main advantages of the electronic circuits thus fabricated are that the highly insulating sapphire substrate of low parasitic capacitance can provide a higher speed, lower power consumption, greater linearity and better insulation (Imthurn, 2007). However, there are some problems associated with the fabrication of such systems, e.g., the high density of crystalline defects and the complex residual stresses. The mismatch of the lattice parameters and of the thermal expansion properties between thin film layers and substrate materials are the main causes of cross-layer defect development and residual stress generation (Nakamura, 2004, Yamamoto, 1979). Several methods have been proposed to minimise the residual stresses caused by lattice mismatch (Lau, 1979), such as ion implantation and annealing (Hull, 1999, Roulet, 1979, Vodenitcharova, 2007) of which the former is to introduce further disorder in the crystalline as-deposited structure and the latter is to regrow the crystalline layers.

Residual stresses in a thin film system are often detrimental to its performance. If sufficiently large, they can lead to buckling, cracking, void formation and film debonding (Freund, 2003, Mei, 2007, Mylvaganam, 2003). Therefore, a complete understanding of the

residual stress generation in relation to fabrication processes is essential. In the past, a great deal of effort has been on the experimental and analytical studies (People, 1985, Tsao, 1987), and has brought about the understanding of energies related to the misfit strain and dislocations. The stress generation mechanism in silicon-on-sapphire (SOS) thin film systems without buffer layers has also been partially investigated. Mavi et al. (1991) used the Raman spectroscopy to measure and compare the localised stresses of annealed, as-deposited and phosphorous ions implanted SOS thin films. To calculate stresses in thin film systems, the Stoney formula (Stoney, 1909) has been commonly used (Brown, 2007, Ha, 2006, Ngo, 2007, Shen, 1996). Feng et al. (2008) and Ngo et al. (2008) extended this formula to calculate the stresses in multi-layered thin films deposited on a substrate subjected to non-uniform misfit strains, which provides a way to determine experimentally the stresses in such systems. Although the analytical and experimental methods, including the wafer curvature (Flinn, 2008, Shen 1996) and X-ray (Flinn, 1988 and 1990) methods, are useful, they have some major disadvantages: (i) they can give only the average and local stresses in a volume; (ii) they cannot provide the stress variation, distribution and directions in a thin film system during fabrication; and (iii) they cannot reveal stress discontinuity across individual layers.

The finite element (FE) method is an efficient technique to attach a complex system (Pramanik, 2007 and 2008), which can be useful to the residual stress analysis of a multi-layered thin film system. Subramaniam et al. (2003) used a two-dimensional FE calculation to understand the threshold thickness where misfit strain between a Si substrate and GeSi

film is partially released by the formation of misfit dislocations. Amaya-Roncancio et al. (2008) used a two-dimensional FE model to investigate the indentation on Cr/CrN multi-layered coatings. Wright et al. (1994) carried out a two-dimensional FE investigation on the residual stresses in diamond thin films caused by cooling from elevated temperatures. In their investigation, however, the materials were assumed to be isotropic and homogeneous. Lee et al. (Lee 1998) also used two-dimensional FE models to calculate the stresses in interconnection structures as a function of process step, such as film deposition, etching, and thermal cycles. Similar to Wright et al. (1994) they considered that all the materials are isotropic. However, they used the strains obtained from experiment using X-ray and curvature methods to induce intrinsic strains in material layers in addition to their thermal mismatch.

As a matter of fact, the two-dimensional FE analyses summarised above cannot provide an accurate understanding of the generation and distribution of residual stresses, because semiconductor materials such as mono-crystalline silicon and sapphire are anisotropic. Unfortunately, a three-dimensional residual stress analysis of SOS systems considering the real material properties is unavailable. This has hindered possible optimization of the SOS fabrication processes with minimised residual stresses. The aim of this paper is to carry out a three-dimensional finite element analysis to fill the gap in this area to provide a relatively complete figure about the residual stress generation in SOS systems.

## 2. Finite element modelling

### 2.1 Element division

A three-dimensional finite element model is shown in Fig. 1. The shape of the model exactly resembles that of a real SOS thin film system to capture the possible shape effect of the wafer geometry, such as the flat edge indicating the wafer's crystallographic plane. This model contains a small volume of the material system at the center of the FE control volume, within which very fine element mesh was used to obtain higher computation accuracy. For convenience, we call this small volume the volume of interest (VOI). Outside the VOI, a coarser FE mesh was constructed to improve computational efficiency. The size of the control volume was five times greater than that of the VOI in Y and Z directions so that the possible boundary effect can be avoided (Zhang, 1996). The dimensions of the VOI are  $0.1\mu\text{m} \times 0.1\mu\text{m} \times 0.34\mu\text{m}$ . The thicknesses of the crystalline silicon thin film, buffer layer and sapphire substrate are  $0.1\mu\text{m}$ ,  $0.04\mu\text{m}$  and  $0.2\mu\text{m}$ , respectively. The VOI contained 4,249 elements whose side length (smallest) was around  $8.3\text{E-}3\mu\text{m}$  (see Fig. 3), whereas the whole control volume consisted of 11,376 elements. The finite element used was the three-dimensional Solid 98 in ANSYS (ANSYS manual) which has ten nodes and six degrees of freedom at each node. This type of element has both the thermal and structural fields and coupling capability required for the present analysis.

## ***2.2 Properties of the SOS materials***

In the fabrication of a multi-layered SOS thin film system, a silicon thin film is normally deposited on to the R-plane of sapphire to minimize the atomic lattice mismatch between the two materials (Nakamura, 2004). Thus in our FE analysis, the sapphire substrate considered was also along its R-plane. According to Vodenitcharova et al. (2007), sapphire in this orientation could be considered as an orthotropic material, whose crystalline planes related to the X, Y and Z axes are illustrated in Fig. 2. The buffer layer was considered to be isotropic due to its amorphous nature. The elastic and thermal properties of silicon layers and sapphire substrate are based on Ref (Hull, 1999, Vodenitcharova, 2007). Table 1 lists the material properties in our FE analysis.

In the analysis at all temperatures, a crystalline structure remains to be crystalline and an amorphous structure maintains its amorphous phase. The deformation of the materials was considered to be elastic and all the material layers were perfectly bonded.

## ***2.3 Boundary and loading conditions***

The thermal and structural boundary conditions, such as the annealing temperature and the buffer layer thickness, were taken from Refs. (Inoue, 1981, Wang, 2000, Vodenitcharova, 2007). The rigid body motion of the control volume (model) was eliminated by fixing some boundary finite element nodes. The nodes at the bottom surface and at the surfaces normal

to z axis were fixed in X and Z directions. A node at the corner of the bottom surface was fixed in Y direction. No structural load was applied, or in other words, the deformation of the system was solely thermal, without mechanically induced forces. The initial temperature of the whole system was 1,000 K, which was consequently cooled down to room temperature (303.15 K) in one hour. A coefficient of convection  $10.45 \text{ w/m}^2\text{K}$  was applied to all the external surfaces of the model (Vodenitcharova, 2007). In the analysis, the thermal and structural fields were coupled.

### **3. Results and discussion**

During the fabrication of a silicon-on-sapphire thin film system, cooling occurs from a high temperature to room temperature to form defect free crystalline silicon thin film on the amorphous silicon (buffer layer). Upon cooling, all layers of the system shrinks. Thus, residual stresses are generated due to dissimilar thermal expansion coefficients of the materials in different directions. Although some studies calculated the fracture and debonding, they assumed that their thin film systems were of isotropic materials and the stress distribution was equi-biaxial (Freund, 2003, Hutchinson, 1996). These assumptions can lead to incorrect stress results; thus it is important to analyse correctly using the anisotropic model described in the present paper.

#### **3.1 Development of von Mises stress**



The von Mises yield criterion has been applied to brittle materials (Brock, 1996, Labbane, 1993, Zhang 1996). Our analysis shows that at the start of the cooling process, the magnitudes of residual stresses (Fig. 4(a)) are small. The highest stress (0.3341 MPa) is found in the crystalline silicon thin film near the interface with the buffer layer. The thickness of the stress contour in the silicon film increases in the positive direction of Z axis. In the buffer layer (amorphous silicon), the highest stress is close to the interface with the sapphire substrate. The stress contours are uniformly distributed with Y and Z. Similar to the silicon film and buffer layer, the stresses in the sapphire substrate are in a layered pattern. In this case, however, the stress contours vary in all directions and create a lowest stress zone around the middle of the VOI.

Upon further cooling, the maximum stress zone moves into the buffer layer close to the interface with the sapphire substrate. The pattern of the stress distribution is similar to that at the initial cooling state although the magnitude of the stress of every contour has increased (Fig. 4(c)). As the cooling continues, the stress level of the contours increases (Fig. 4(d)). After cooling down to 303.184K, the highest residual von Mises stress is found to be in the buffer layer near the interface with the sapphire substrate, with a magnitude of 240.6 MPa. The maximum stresses in the silicon thin film, the buffer layer and the sapphire substrate are 148.33, 240.622 and 194.478 MPa, respectively. Thus the defects may initiate at the highest stress zone if the stress is high enough.

### 3.2 Development of von-Mises strain

During the cooling process, the distribution of von Mises strain is almost similar to that of von Mises stress. The maximum strain is found to be in the buffer layer from the start of cooling. The magnitude of strain increases throughout the cooling. At different locations in the sapphire substrate, the variation of strain at a given temperature is small. At the end of the cooling, the maximum strain is 0.002126 and is in the buffer layer near the interface with the sapphire substrate.

### 3.3 Distribution of normal stresses

In this section, the distributions and directions of the normal stresses in the multi-layered thin film system will be discussed. In doing so, two cross-sectional planes of the VOI are chosen based on the XYZ coordinate system in Fig. 2, where one is (001), which is normal to the Z-axis located at  $0.05\mu\text{m}$  from the centre of the model, and the other is (010), which is normal to the Y-axis located at  $0.05\mu\text{m}$  from the centre. The stresses at several points on each of the above cross-sectional planes are analysed. The approximate locations of these points such as A, B, C, D1, D2, E, F1, F2, G, H and I are shown in Fig. 5. Points D (D1- in the silicon thin film, D2- in the buffer layer) and F (F1- in the buffer layer, F2- in the sapphire substrate) are located on the interfaces of thin film/buffer layer and buffer layer/sapphire substrate respectively.

### 3.3.1 Normal stresses at the cross-section in the (001) plane

The maximum normal stress (the first principal stress) increases with the decrease in temperature (Fig. 6). The increase of stresses is not uniform at all the points denoted in Fig. 5. The stress at Point A in the silicon thin film does not have a noticeable variation during cooling. However, the normal stress increases in the depth of the thin film but experiences a discontinuity of a tiny decrease at the interface with the buffer layer (From Point D1 to D2). This is caused by the sudden property change from the thin film to the buffer layer. Inside the buffer layer, the stress rises again until reaching the interface with the sapphire substrate. A sudden jump of the stress (stress discontinuity) occurs across the interface from Point F1 to F2. Such a sharp stress change can lead to interface debonding if the stress is sufficiently large (Zhang, 1996). The maximum stress is at Point F2 in the sapphire substrate. After passing the F1/F2 interface, the stress decreases in the sapphire substrate.

The variation of the minimum normal stresses (the third principal stress) in the multi-layered thin film system is shown in Fig. 7. It can be seen that they are compressive inside the silicon thin film and buffer layer but become tensile in the sapphire substrate. The compressive stresses toward the D1/D2 interface increase gradually, but rise sharply across the interface. An even more significant jump of the stresses occurs at the interface from the buffer layer to the sapphire substrate (from point F1 to F2). This can bring about film buckling/wrinkling or debonding if the stresses are big enough (Evans, 2007, Littenken,

2005, Mogilyanski, 2000). After the F1/F2 interface, the stresses decrease inside the sapphire substrate.

The directions and distributions of the maximum and minimum normal stresses are presented in Figs. 8 and 9, respectively. In the case of the maximum normal stresses, Fig. 8 shows that at different locations their directions change, which are parallel with the X-axis at the bottom part of the sapphire substrate but become almost parallel with the Y-axis near the interface with the buffer layer. The stresses in other parts of the thin film system are almost in parallel with the X-axis. The stress directions do not have noticeable changes during the whole cooling process.

Unlike the maximum normal stresses, the directions of the minimum normal stresses vary in cooling. Initially, stresses are parallel with the Z-axis at the bottom part of the sapphire. Their directions then rotate to have small angles with the Z-axis when approaching the interface with the buffer layer (Fig. 9(a)). Upon further cooling (Fig. 9(b)), the stresses in the sapphire tend to be parallel with the X-axis. On the other hand, the stresses in the thin film and buffer layer are parallel with the XY-plane at an angle of 45 degrees (approximately) with the X- or Y-axis. The directions of these stresses remain unchanged during further cooling (Fig. 9(c)).

The change of the normal stress directions at different locations in the system may cause damages during the cooling process (Zhang, 1996).

### 3.3.2 Normal stresses at the cross-section in (010) plane

To examine the anisotropy effect of the crystalline silicon thin film and the sapphire substrate, the normal stress distributions in another cross-sectional plane (010) are analysed. Figs. 10 and 11 show the maximum and minimum normal stresses in this plane. Qualitatively, the stress variation is similar to that in the (001) plane discussed previously. The maximum normal stresses in plane (010) are slightly higher than those in the (001) plane. Stress discontinuity also exists across the interfaces from F1 to F2 (Figs. 10 & 11) and from D1 to D2 (Fig. 11).

The directions of the maximum normal stresses are parallel with the X-axis at the bottom part of the sapphire substrate (Fig. 12(a)) and remain unchanged until the end of the cooling process (Fig. 12(c)); but the stresses close to the interface with the buffer layer are not in parallel with any axis. These are in XZ-plane with a small angle with the X-axis and the angle increases until reaching a certain temperature. The angle then remains constant till the end of the cooling (Fig. 12(c)).

On the other hand, at the initial stage of cooling the minimum normal stresses at the bottom of sapphire substrate are parallel with the Z-axis and in the neighbourhood of the interface (top) they turn to form an angle with respect to the Z-axis (Fig. 13), until the end of the cooling (Figs. 13(a)-(c)). The stresses in the thin film and buffer layer are mostly parallel with the YZ-plane throughout the cooling process (Figs. 13(a)-(c)).

### 3.4 Fracture and buckling of thin film

There are many investigations in thin film production and improvement as mentioned earlier. It is well known that residual stresses are responsible for thin film delamination and, film and/or substrate fracture. In reference (Freund, 2003) biaxial residual stresses (in plane and parallel of thin film) have been correlated with fracture energy of thin film by using Griffith's theory of fracture with a consideration of stress discontinuity at the interfaces. Hence, residual stresses in axial directions will be discussed in this section to get some practical insight of defect formation in thin films.

From our discussion in previous sections, we see that axial stresses increase with the decrease of temperature at every interface. Stresses are relatively low at the top surface of the film. In Z direction, the compressive stresses are in the range of -29.9 to -79MPa. Tensile and compressive stresses are noted in the range of 8.5 to -5.3MPa in the Y direction. With the increase of depth of the film, the stresses increase. At the bottom of the film, the stresses are in the range of -58.23 to -59.7MPa and -48.36 to -58.54MPa in Y and Z direction respectively. On the other hand, the stresses in the buffer layer at the interface

with the thin film are in the range of -59.02 to -61.78MPa and -71.5 to -86.04MPa in Y and Z directions. A tensile stress (21.13 to 18.58MPa) is found in the X direction at this interface. The stress discontinuity at the interface between the film and the buffer layer is not significant in Y direction but is high in Z direction.

The stresses in the buffer layer vary significantly from its top surface to its bottom. The compressive stresses are in the ranges of -166.11 to -170.42MPa and -171.12 to -181.21 MPa in Y and Z directions respectively at the bottom of the buffer layer. In contrast, tensile stresses in the ranges of 247.23 to 231.02MPa and 211.5 to 178.67MPa are noted in the Y and Z directions respectively, in the top surface of sapphire substrate (at the interface with buffer layer). Tensile stresses in the range of 61.82 to 56.32MPa are found in the X direction at interface (buffer layer/substrate). These cause a significant stress discontinuity at the buffer layer/sapphire interface.

From the above discussion it is clear that the thin film and buffer layer are mostly in compression at room temperature. On the other hand, sapphire substrate is under very high tension. At both the interfaces, tensile stresses are normal to the faces. According to reference (Freund, 2003), these may initiate delamination at the film/buffer layer interface and, fracture and delamination at the buffer layer/sapphire substrate interface if stresses are high enough. In addition, the stress gradient in every layers of the system may further promote delamination (Chai, 1990).

### 3.5 Effect of buffer layer thickness

As mentioned earlier, an amorphous silicon layer is introduced between the crystalline silicon film and the sapphire substrate as a buffer layer in the thin film system to reduce the possible residual stress magnitude. The mechanism is to use the amorphous nature of the buffer layer to minimise the mismatch of the crystalline lattice structures of different materials. Hence, the thickness of the buffer layer must play an important role in the stress generation and distribution in a multi-layered thin film system. In this section we will investigate the thickness effect of the buffer layer by examining the stress variations with different thickness of 0.4, 0.6, 0.8 and 1 $\mu\text{m}$ .

The distribution of the von Mises stresses in the VOI for different thickness of buffer layer is presented in Fig. 14. It is interesting to note that the stress contours of higher magnitudes in the thin film move towards/into the buffer layer with the increase of the thickness. The highest stress in the thin film is around 195MPa (Fig. 14(a)) when the buffer layer thickness is 0.4 $\mu\text{m}$  but decreases to 123MPa (Fig. 14(d)) when the buffer layer thickness becomes 0.1 $\mu\text{m}$ .

The maximum normal stresses at Points D1, D2, F1 and F2 (Fig. 5) for different buffer layer thicknesses at (001) plane are shown in Fig. 15. At Points D1 and D2 (interface between silicon thin film and buffer layer), there is a significant decrease of stresses with



the increase of the buffer layer thickness after complete cooling. However, the influence of the buffer layer thickness on the stresses is negligible when the temperature is still high (e.g., at 979.423K at the initial stage of cooling). At the interface between the buffer layer and the sapphire substrate (Points F1 and F2), the maximum normal stress decreases with the increase of the buffer layer thickness after complete cooling.

The variation of the minimum normal stresses at Points D1, D2, F1 and F2 with different buffer layer thicknesses is similar to that of maximum normal stresses described above.

#### **4. Conclusions**

The major conclusions from this study are as follows:

- (a) The von Mises stress concentration in the buffer layer near the interface with the sapphire substrate may initiate fracture.
- (b) The stress discontinuity across the interface between the buffer layer and the sapphire substrate is more significant than that cross the interface between the silicon thin film and the buffer layer. This indicates that defects are more likely to be initiated at the interface between the buffer layer and the sapphire substrate.
- (c) The sharp changes of the tensile residual stresses at the interfaces can cause catastrophic failure of thin films if the magnitudes of the stresses are big enough. The

compressive stresses in different layers may cause film buckling/wrinkling if they reach a threshold value.

- (d) The change of directions of the normal stresses in the system may cause damages in the middle of the processing.
- (e) The tensile and compressive residual stresses in a thin film can be greatly reduced when the buffer layer thickness is increased.

### **Acknowledgements**

This work was supported by an ARC Linkage grant and Saphicon Semiconductor. The contribution by A. Brawley, P. Atanackovic and S. Duvall is very much appreciated

### **References**

- Amaya-Roncancio, S., Restrepo-Parra, E., 2008, Finite elements modeling of multilayers of Cr/CrN, *Journal of Microelectron.* 39, 1336–1338.
- ANSYS reference manual, Release 10, ANSYS, Inc., Southpointe 275 Technology Drive Canonsburg, PA 15317, United States, <http://www.ansys.com>
- Brock, L. M., 1996, Effects of thermoelasticity and a von mises condition in rapid steady-state quasi-brittle fracture, *International Journal of Solids and Structures* 33 (28), 4131-4142.

- Brown, M.A., Rosakis, A.J., Feng, X., Huang, Y., Üstündag, E., 2007, Thin film/substrate systems featuring arbitrary film thickness and misfit strain distributions. Part II: Experimental validation of the non-local stress/curvature relations, *International Journal of Solids and Structures* 44, 1755–1767.
- Chai, H., 1990, Three-dimensional fracture analysis of thin-film debonding, *International Journal of Fracture* 46, 237-256.
- Evans, A.G., Hutchinson, J.W., 2007, The mechanics of coating delamination in thermal gradients, *Surface & Coatings Technology* 201, 7905–7916.
- Feng, X., Huang, Y., Rosakis, A.J., 2008, Multi-layer thin films/substrate system subjected to non-uniform misfit strains, *International Journal of Solids and Structures* 45, 3688–3698.
- Flinn, P.A., Waychunas, G.A., 1988, A new x-ray diffractometer design for thin-film texture, strain, and phase characterization, *J. Vac. Sci. Technol. B* 6, 1749–1755.
- Flinn, P.A., Chiang, C., 1990, X-ray diffraction determination of the effect of various passivations on stress in metal films and patterned lines, *J. Appl. Phys.* 67, 2927–2931.
- Flinn, P.A., 2008, Thin Films: Stress Measurement Techniques, *Encyclopaedia of Materials: Science and Technology* 9274-9279.
- Freund, L.B., Suresh, S., 2003, *Thin film materials: stress, defect formation and surface evolution*, Cambridge, U.K.; New York : Cambridge University Press.
- Ha, P.C.T., McKenzie, D.R., Bilek, M.M.M., Doyle, E.D., McCulloch, D.G., Chu, P.K., 2006, Control of stress and delamination in single and multi-layer carbon thin films

- prepared by cathodic arc and RF plasma deposition and implantation, *Surface & Coatings Technology* 200, 6405–6408.
- Hull, R., 1999, *Properties of crystalline silicon*, Publisher: INSPEC, the Institution of Electrical Engineers, London.
- Hutchinson, J.W., 1996, *Mechanics of thin films and multi-layers: Course Notes*, Technical University of Denmark, Technical Report.
- Imthurn, G., 2007, *The History of Silicon-on-Sapphire*, available at [http://www.peregrine-semi.com/articles/History\\_SOS\\_73-0020-02.pdf](http://www.peregrine-semi.com/articles/History_SOS_73-0020-02.pdf)
- Inoue, T., Yoshii, T., 1981, Crystalline quality improvement of SOS films by Si implantation and subsequent annealing, *Nuclear Instruments and Methods* 182-183, 683-690.
- Labbane, M., Saha, N.K., Ting E.C., 1993, Yield criterion and loading function for concrete plasticity, *International Journal of Solids and Structures* 30 (9), 1269- 1288.
- Lau, S.S., Matteson, S., Mayer, J.W., Revez, P., Gyulai, J., Roth, J., Sigmon, T.W., Cass, T., 1979, Improvement of crystalline quality of epitaxial Si layers by ion-implantation techniques, *Appl. Phys. Lett.* 34, 76.
- Lee, J., Mack, A.S., 1998, Finite element simulation of a stress history during the manufacturing process of thin film stacks in VLSI structures, *IEEE Transactions on semiconductor manufacturing* 11(3), 458-464.
- Litteken, C.S., Strohsand, S., Dauskardt, R.H., 2005, Residual stress effects on plastic deformation and interfacial fracture in thin-film structures, *Acta Materialia* 53, 1955–1961.

- Mavi, H.S., Shukla, A.K., Jain, K.P., Abbi, S.C., Beserman, R., 1991, Raman study of stress-relieved silicon-on-sapphire films prepared by cw-laser annealing, *J. Appl. Phys.* 69 (11), 7815-7819.
- McCann, M.J., Catchpole, K.R., Weber, K.J., Blakers, A.W., 2001, A review of thin-film crystalline silicon for solar cell applications. Part 1: Native substrates, *Solar Energy Materials & Solar Cells* 68, 135-171.
- Mei, H., An, J.H., Huang, R., Ferreira, P.J., 2007, Finite element modeling of stress variation in multilayer thin-film specimens for in situ transmission electron microscopy experiments, *Journal of Materials Research* 22 (10), 2737-2741
- Mogilyanski, D., Gartstein, E., Metzger, H., 2000, Characterization of the interface strain/stress state in Si-on-Sapphire heterostructure, *Materials Science Forum* 347-349, 568-573.
- Mylvaganam, K., Zhang, L.C., 2003, Residual stress induced atomic scale buckling of diamond carbon coatings on silicon substrate, *Thin Solid Films* 425, 145–149.
- Ngo, D., Feng, X., Huang, Y., Rosakis, A.J., Brown, M.A., 2007, Thin film/substrate systems featuring arbitrary film thickness and misfit strain distributions. Part I: Analysis for obtaining film stress from non-local curvature information, *International Journal of Solids and Structures* 44, 1745–1754.
- Ngo, D., Feng, X., Huang, Y., Rosakis, A.J., 2008, Multilayer thin films/substrate system with variable film thickness subjected to non-uniform misfit strains, *Acta Materialia* 56, 5322–5328.

- People, R., Bean, J.C., 1985, Calculation of critical layer thickness versus lattice mismatch for  $\text{Ge}_x\text{Si}_{1-x}/\text{Si}$  strained-layer heterostructures, *Appl. Phys. Lett.* 47, 322–324.
- Pramanik, A., Zhang, L.C., Arsecularatne, J.A., 2007, An FEM investigation into the behaviour of metal matrix composites: tool–particle interaction during orthogonal cutting, *International Journal of Machine Tools & Manufacture* 47, 1497–1506.
- Pramanik, A., Neo, K.S., Rahman, M., Li, X.P., Sawa, M., Maeda, Y., 2008a, *Journal of materials processing technology* 208, 400–408.
- Pramanik, A., Zhang, L.C., Arsecularatne, J.A., 2008, Deformation mechanisms of MMCs under indentation, *Composites Science and Technology* 68, 1304–1312.
- Richmond, E.D., Knudson, A.R., 1982, New developments in the defect structure of implanted furnace-annealed silicon on sapphire, *Thin Solid Films* 93, 347-351.
- Roulet, M.E., Schwob, P., Affolter, K., Luthy, W., Yon Atlmen, M., Fallavier, M., Mackowski, J.M., Nicolet, M.A., Thomas, J.P., 1979, Laser annealing of silicon on sapphire, *J. Appl. Phys.* 50, 5536.
- Shen, Y.L., Suresh, S., Blech, I.A., 1996, Stresses, curvatures, and shape changes arising from patterned lines on silicon wafers, *J. Appl. Phys.* 80, 1388-1398.
- Stoney, G.G., 1909, The tension of metallic films deposited by electrolysis, *Proc. R. Soc. Lond.* A82, 172–175.
- Subramaniam, A., Ramakrishnan, N., 2003, Analysis of thin film growth using finite element method, *Surface and Coatings Technology* 167, 249–254.

- T. Nakamura, H. Matsubishi, Y. Nagatomo, 2004, Silicon on Sapphire (SOS) Device Technology, Oki Technical Review, Technologies that Support the e-Society 71(200)(4), <http://www.oki.com/en/otr/200/downloads/otr-200-R18.pdf>
- Tsao, J.Y., Dodson, B.W., Picraux, S.T., Cornelison, D.M., 1987, Critical stresses for  $\text{Si}_x\text{Ge}_{1-x}$  strained-layer plasticity, *Phys. Rev. Lett.* 59, 2455–2458.
- Vodenitcharova, T., Zhang, L.C., Zarudi, I., Yin, Y., Domyo, H., Ho, T., Sato, M., 2007, The effect of anisotropy on the deformation and fracture of sapphire wafers subjected to thermal shocks, *Journal of Materials Processing Technology* 194(1-3), 52-62.
- Wang, Q., Nie, J., Yu, F., Liu, Z., Yu, Y., 2000, Improvement of thin silicon on sapphire (SOS) film materials and device performances by solid phase epitaxy, *Materials Science and Engineering B72*, 189–192.
- Wright, J.K., Williamson, R.L., Maggs, K.J., 1994, Finite element analysis of the effectiveness of interlayers in reducing thermal residual stresses in diamond films, *Materials Science and Engineering A* 187, 87-96.
- Yamamoto, Y., Wilson, I.H., and Itoh, T., 1979, Gettering effect by oxygen implantation in SOS, *Appl. Phys. Lett.* 34, 403.
- Zhang, L.C., Mahdi, M., 1996, The plastic behaviour of silicon subjected to micro-indentation, *Journal of Material Science* 31, 5671–5676.

## List of table and figures

Table 1. Properties of materials used in finite element analysis

Fig. 1. The geometrical model of a multilayered thin film system: (a) volume of interest, and (b) the full control volume for the finite element analysis.

Fig. 2. The finite element mesh of the SOS system. (a) volume of interest and (b) the whole control volume.

Fig. 3. The anisotropy of a monocrystalline sapphire [9]. (a) coordinate systems in the sapphire crystal and the R-plane, and (b) a sapphire wafer in the R-plane and the coordinate system in the FEA simulations [10].

Fig. 4. The distribution of the von Mises stress in the VOI at different temperature during the cooling process (in 3600 sec).

Fig. 5. Indication of positions of points for studying the normal stresses on the cross-sectional planes of the VOI.

Fig. 6. The variation of the maximum normal stresses in the thin film system in the (001) plane.

Fig. 7. The minimum normal stress in the thin film system in the (001) plane.

Fig. 8. Directions of the maximum normal stresses in the (001) plane.

Fig. 9. Directions of the minimum normal stresses in the (001) plane.

Fig. 10. The maximum normal stresses in the thin film system in the (010) plane.

Fig. 11. The minimum normal stresses in the thin film system in the (010) plane.

Fig. 12. The directions of the maximum normal stresses in the (010) plane.

Fig. 13. The directions of the minimum normal stresses in the (010) plane.

Fig. 14. Variation of the von Mises stress distribution with the buffer layer thickness at 303.407K.



Fig. 15. Effect of buffer layer thickness on the maximum normal stress in the (001) plane.

Table 1. Properties of materials used in finite element analysis

	Sapphire	Crystalline Silicon	Amorphous Silicon
Modulus of elasticity (GPa)	$E_{xx} = 386$ $E_{yy} = 381.88$ $E_{zz} = 381.88$	$E_{xx} = 79$ $E_{yy} = 130$ $E_{zz} = 130$	113.2
Poisson's ratio	$\mu_{xy} = 0.24$ $\mu_{yz} = 0.25$ $\mu_{zx} = 0.24$	$\mu_{xy} = 0.17$ $\mu_{yz} = 0.28$ $\mu_{zx} = 0.17$	0.20
Specific heat (J/KgK)	800	713	713
Thermal expansion coefficient (1/K)	Parallel to R-plane = 5.04E-6 Normal to R-plane = 4.95E-6	2.55E-6	2.55E-6
Thermal conductivity (W/mK)	46	156	156
Density (kg/mm <sup>3</sup> )	3.98E-5	2.33E-5	2.33E-5

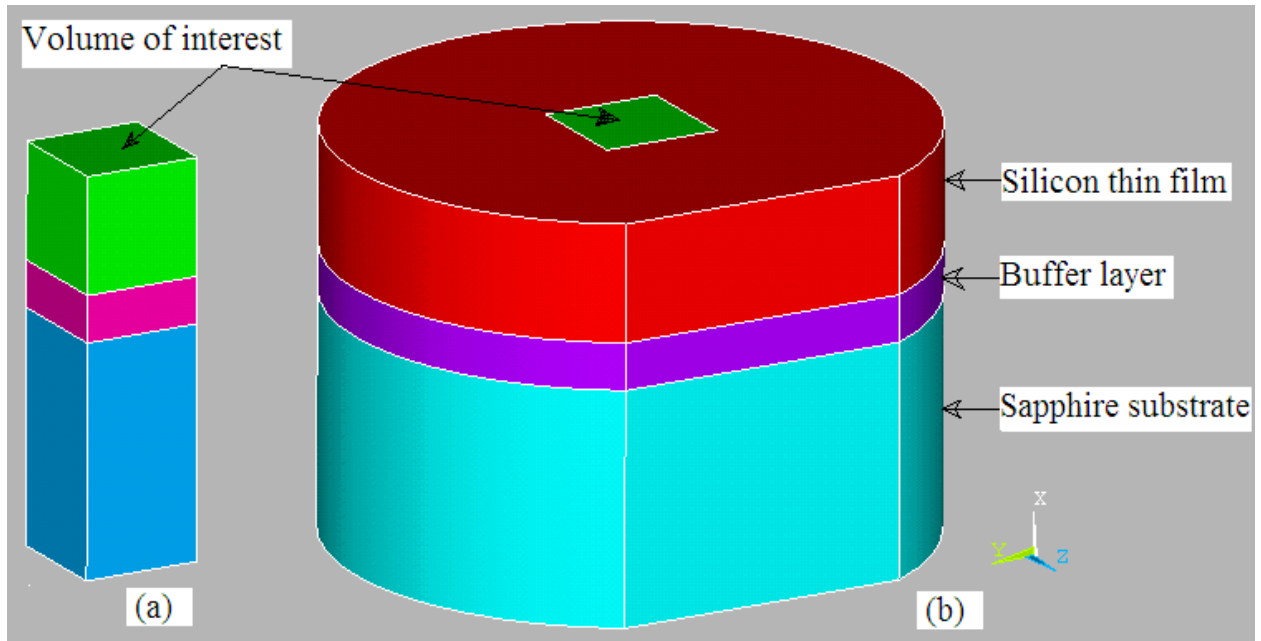


Fig. 1. The geometrical model of a multilayered thin film system: (a) volume of interest, and (b) the full control volume for the finite element analysis.

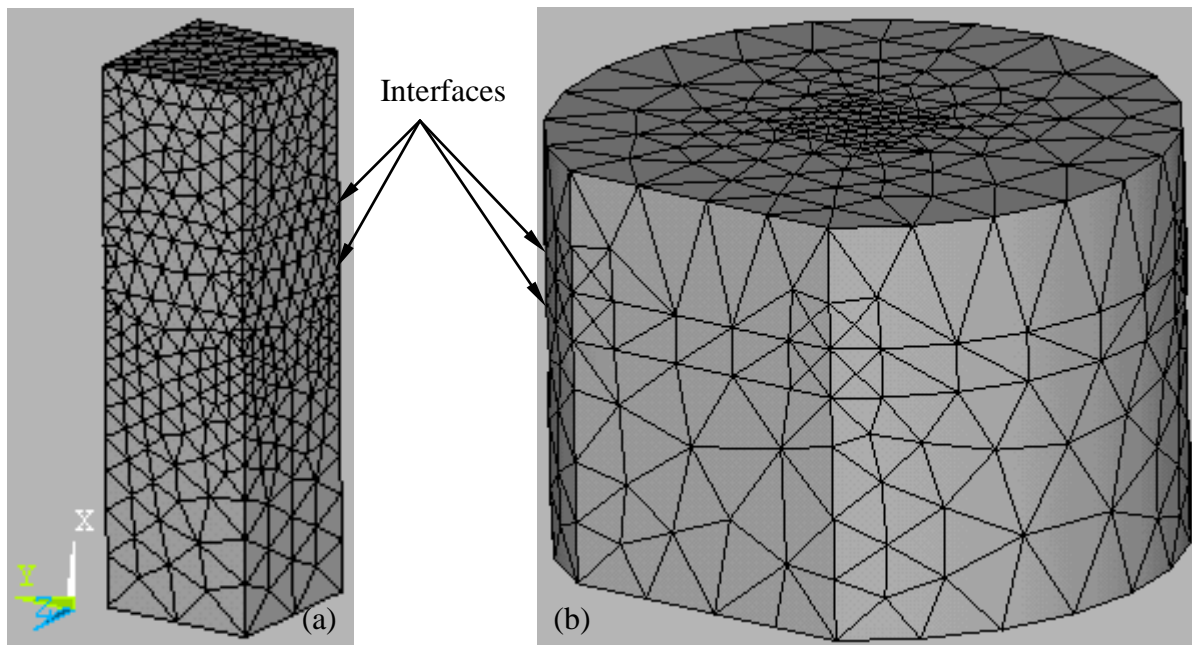


Fig. 2. The finite element mesh of the SOS system. (a) volume of interest and (b) the whole control volume.

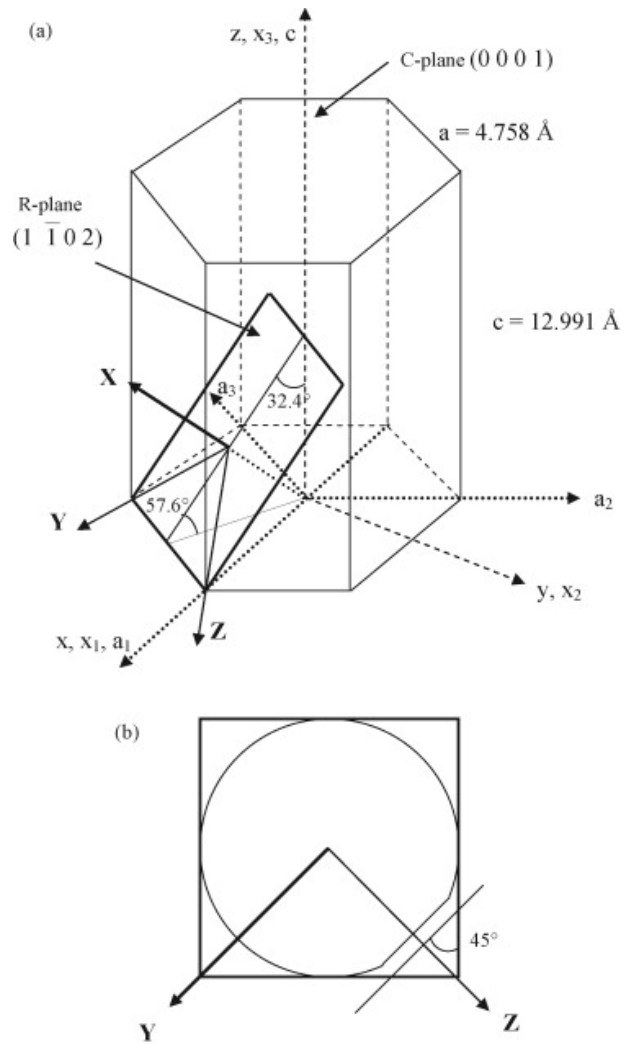


Fig. 3. The anisotropy of a monocrystalline sapphire [9]. (a) coordinate systems in the sapphire crystal and the R-plane, and (b) a sapphire wafer in the R-plane and the coordinate system in the FEA simulations (Vodenitcharova, 2007).

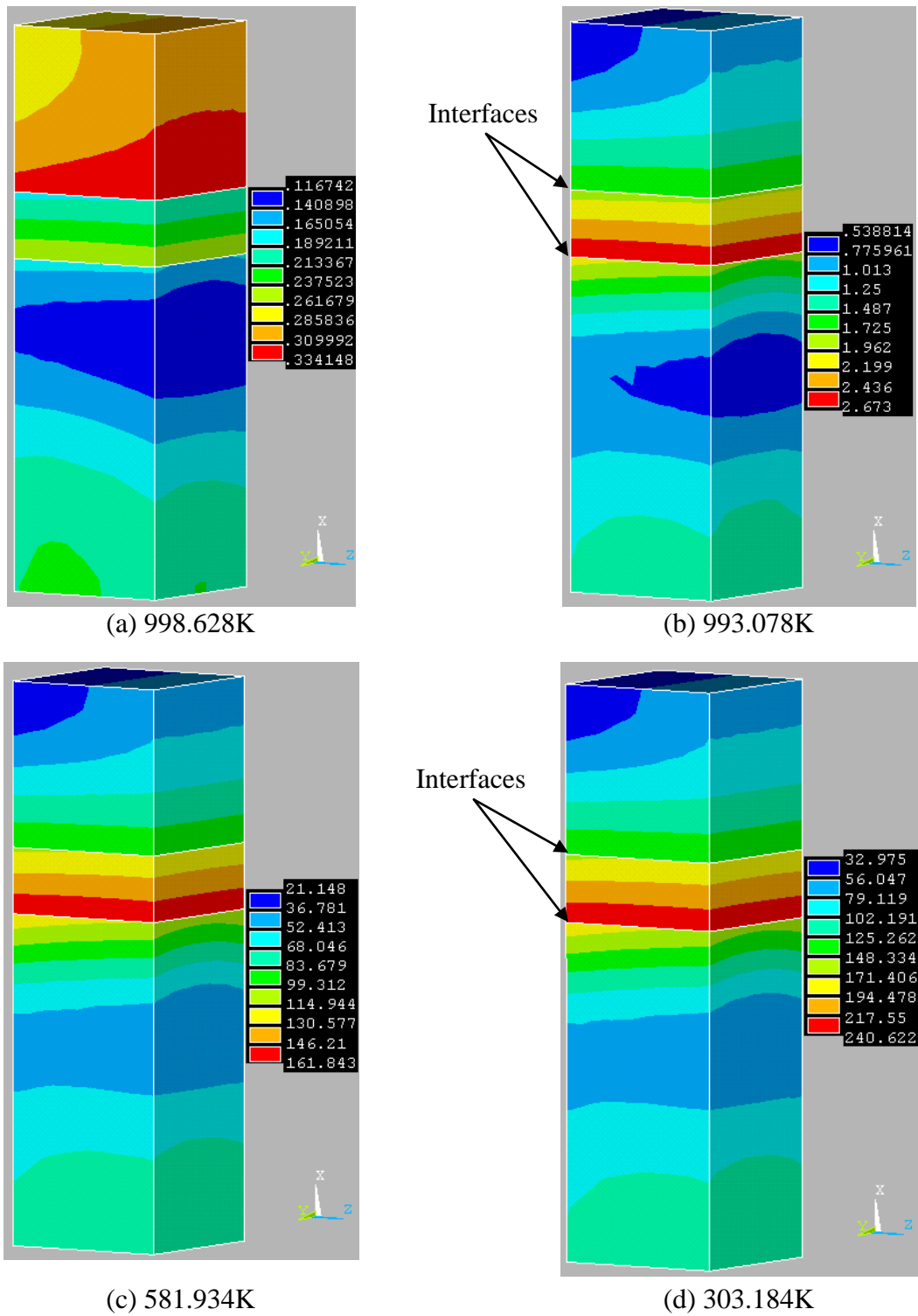


Fig. 4. The distribution of the von Mises stress in the VOI at different temperature during the cooling process (in 3600 sec).

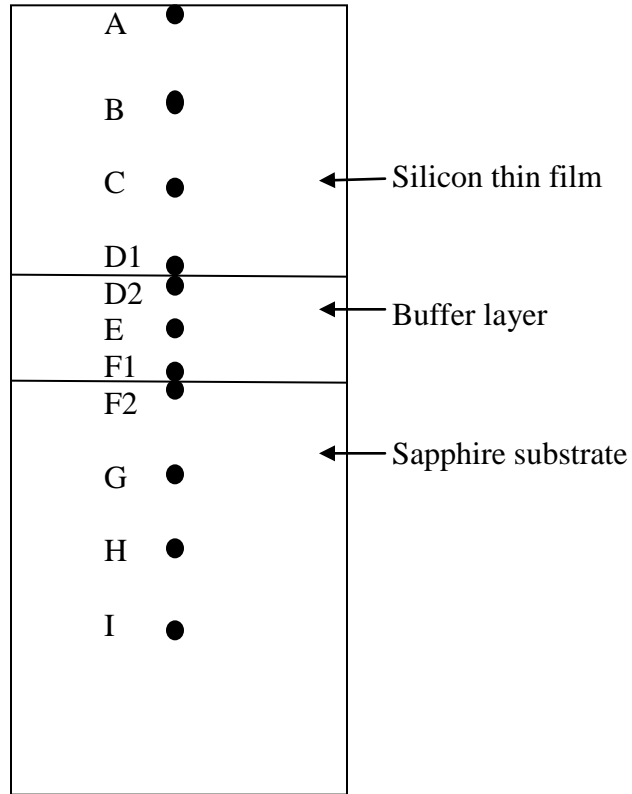


Fig. 5. Indication of positions of points for studying the normal stresses on the cross-sectional planes of the VOI.

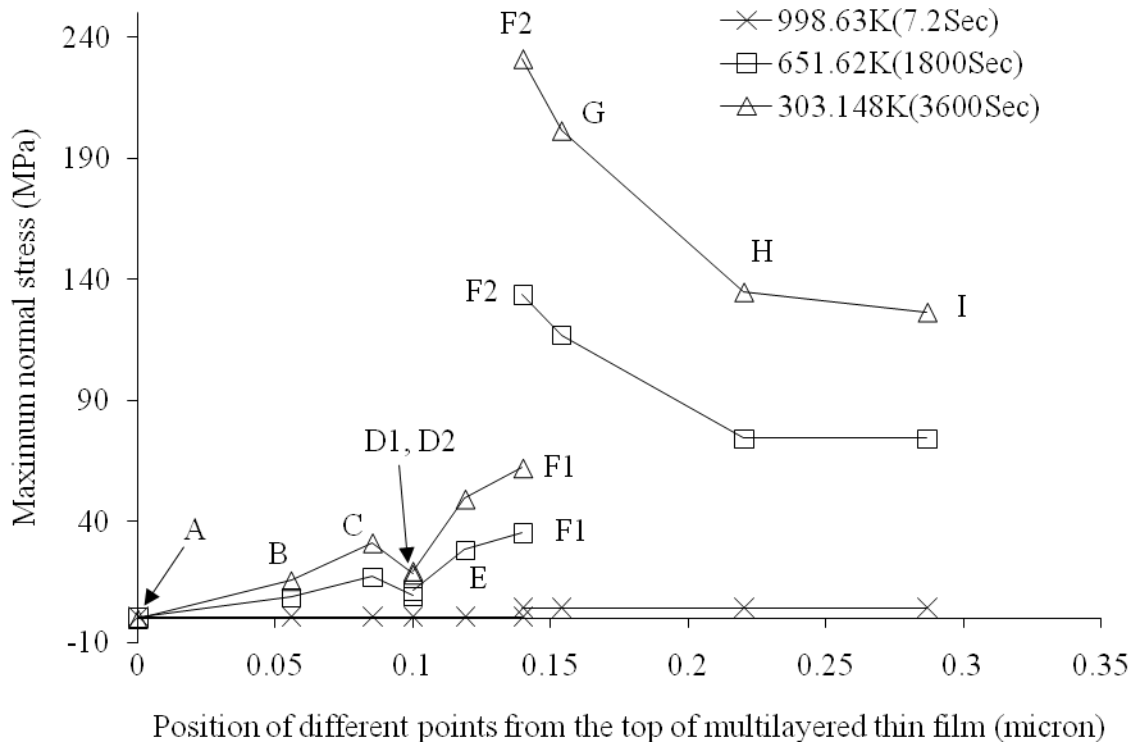


Fig. 6. The variation of the maximum normal stresses in the thin film system in the (001) plane.

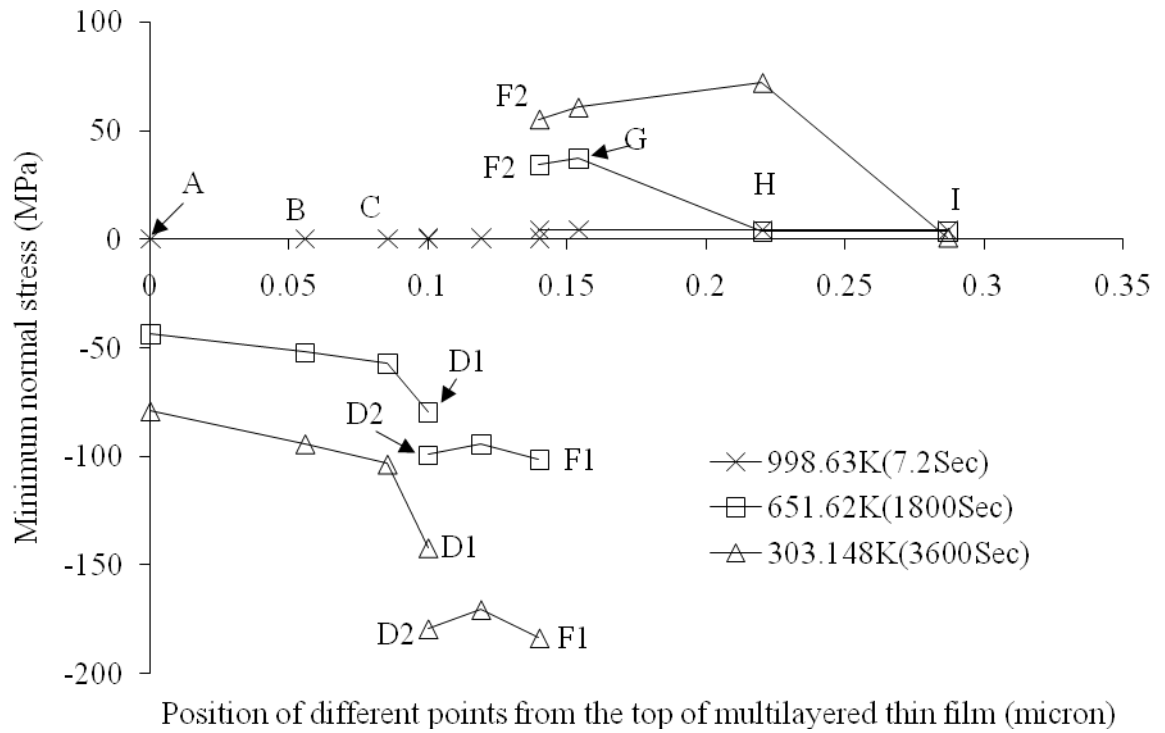


Fig. 7. The minimum normal stress in the thin film system in the (001) plane.

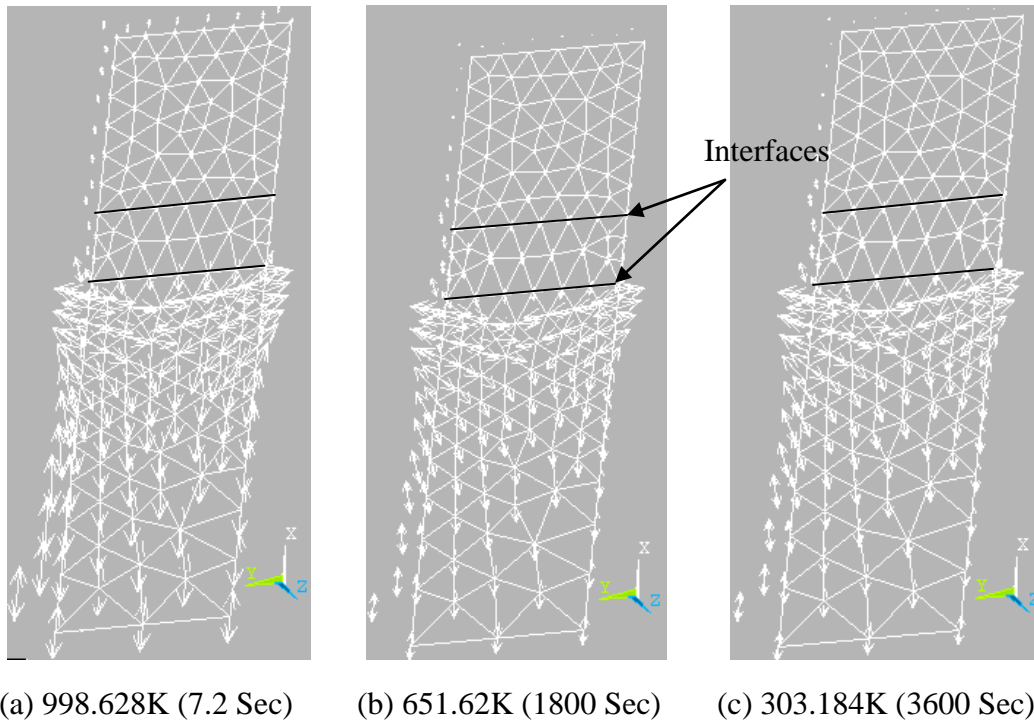


Fig. 8. Directions of the maximum normal stresses in the (001) plane.

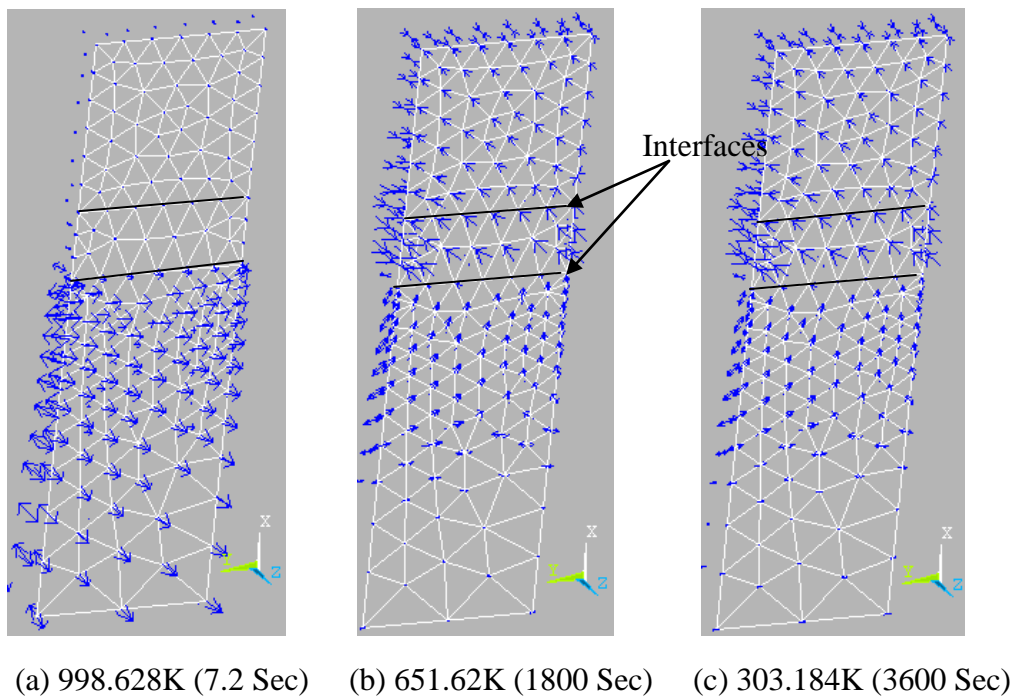


Fig. 9. Directions of the minimum normal stresses in the (001) plane.



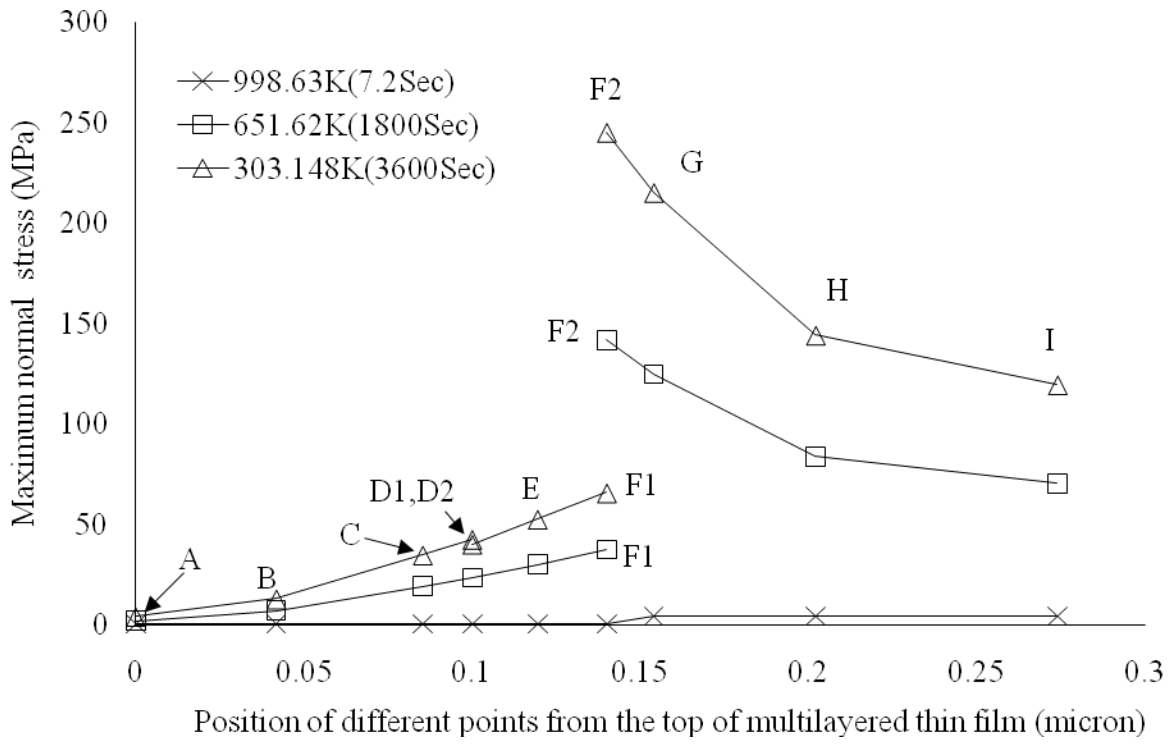


Fig. 10. The maximum normal stresses in the thin film system in the (010) plane.

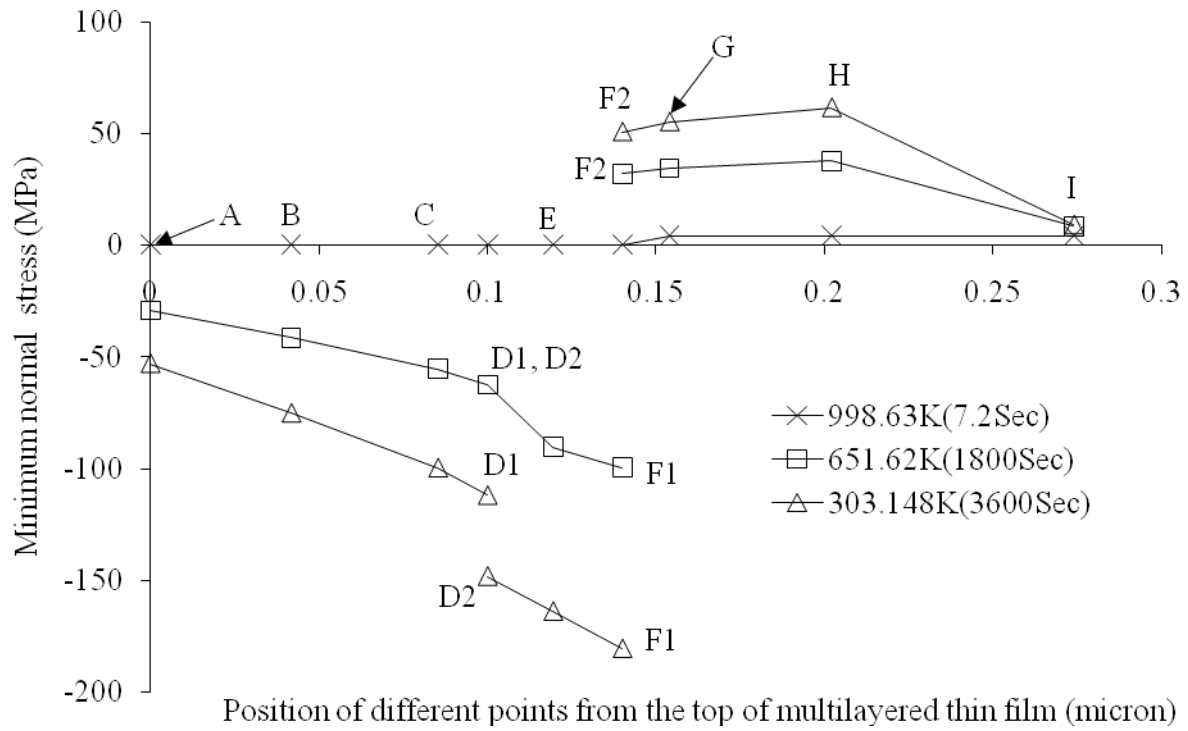
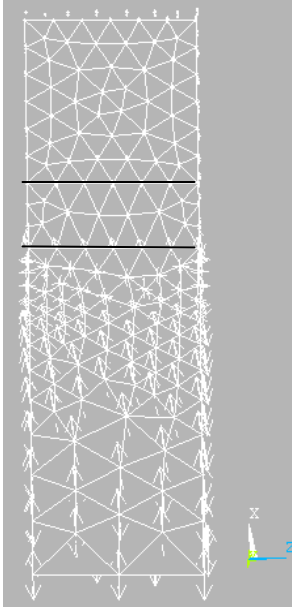
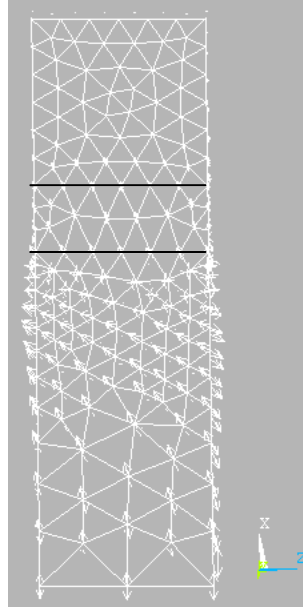


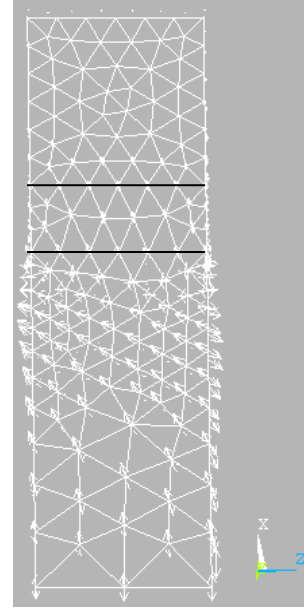
Fig. 11. The minimum normal stresses in the thin film system in the (010) plane.



(a) 998.628K (7.2 Sec)

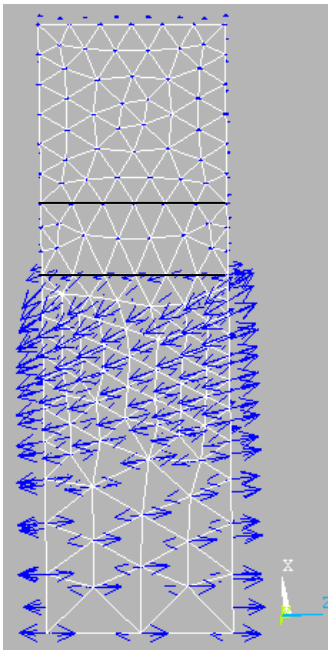


(b) 651.62K (1800 Sec)

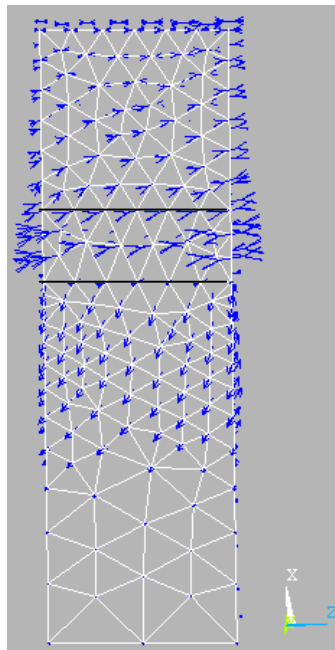


(c) 303.184K (3600 Sec)

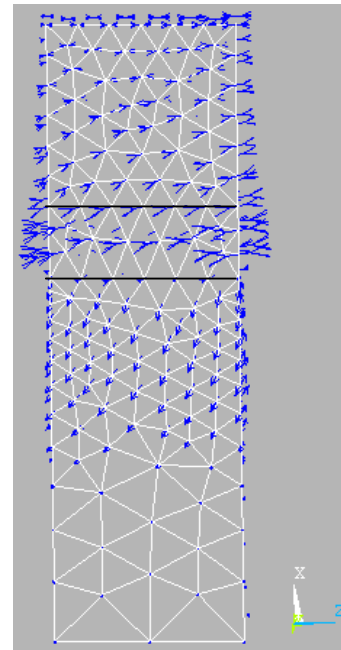
Fig. 12. The directions of the maximum normal stresses in the (010) plane.



(a) 998.628K (7.2 Sec)

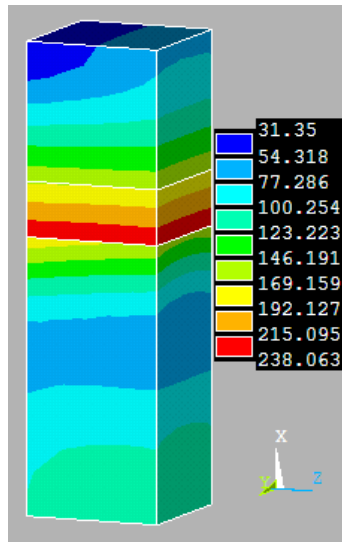


(b) 651.62K (1800 Sec)

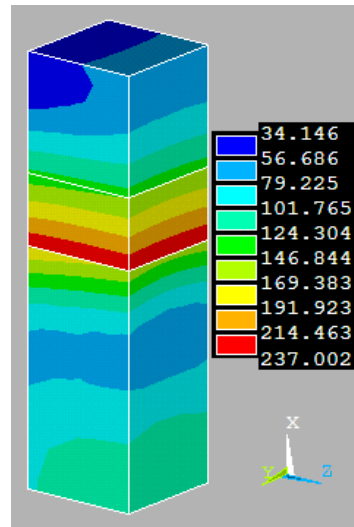


(c) 303.184K (3600 Sec)

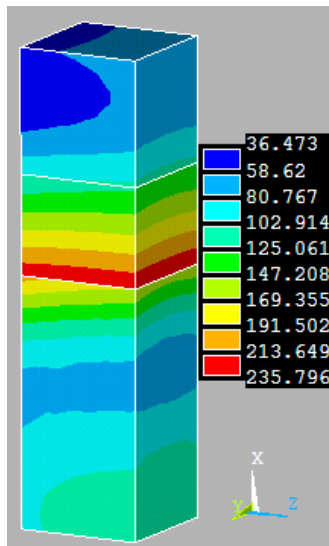
Fig. 13. The directions of the minimum normal stresses in the (010) plane.



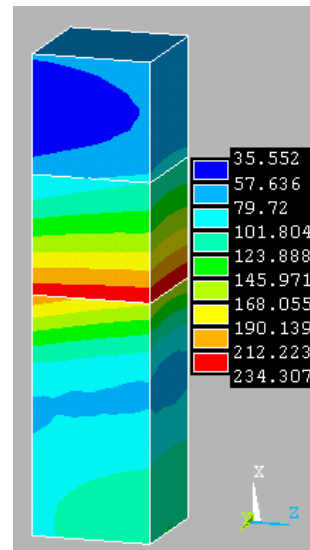
(a) 0.04 $\mu\text{m}$



(b) 0.06 $\mu\text{m}$

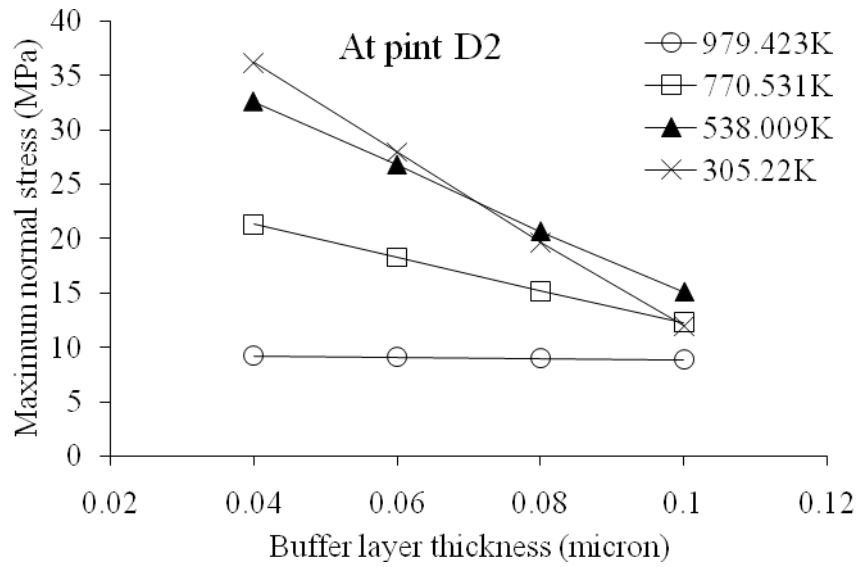
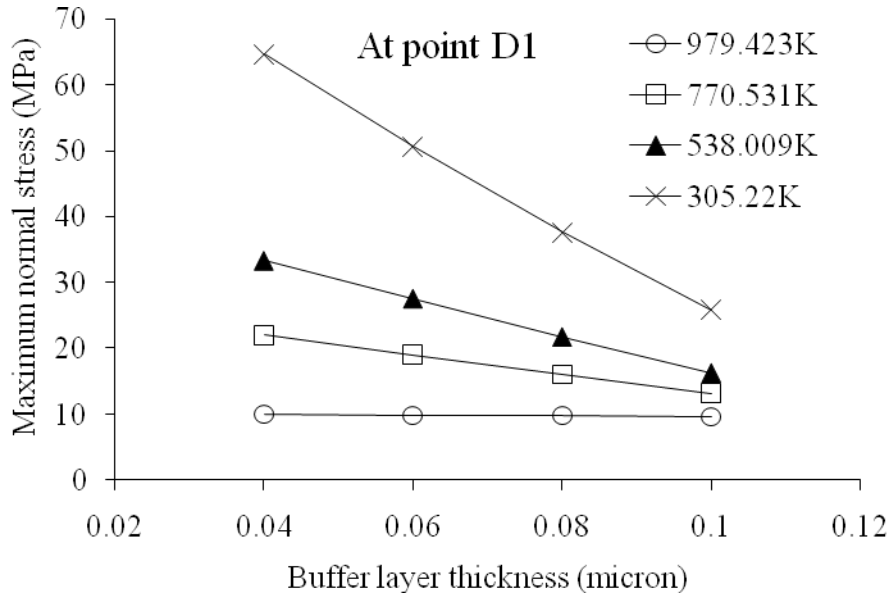


(c) 0.08 $\mu\text{m}$



(d) 0.1 $\mu\text{m}$

Fig. 14. Variation of the von Mises stress distribution with the buffer layer thickness at 303.407K.



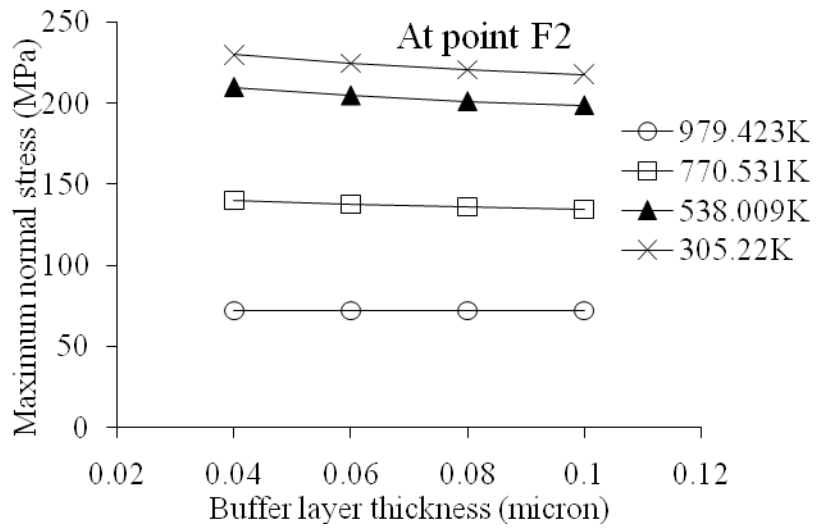
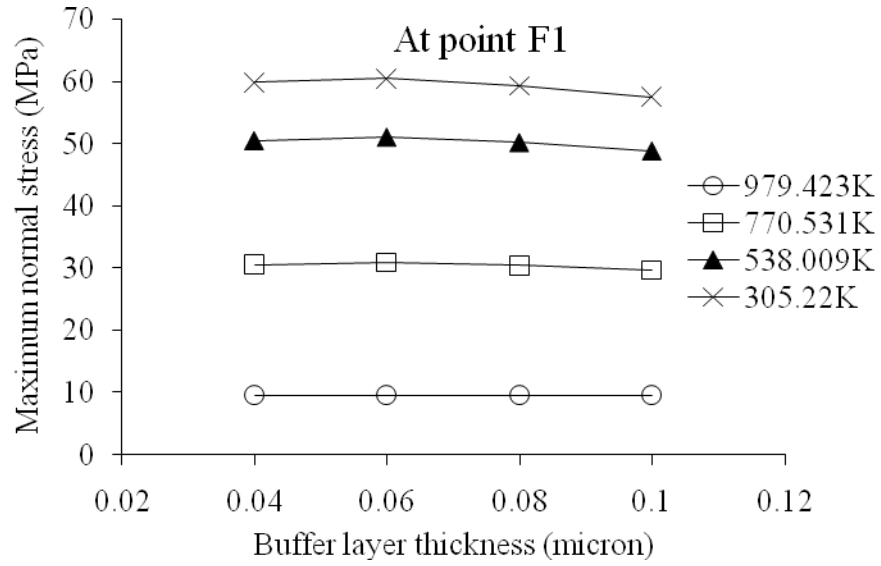


Fig. 15. Effect of buffer layer thickness on the maximum normal stress in the (001) plane.